

Microstructure and mechanical properties of magnesium containing high volume fractions of yttria dispersoids

B.Q. Han, D.C. Dunand *

Department of Materials Science and Engineering, Northwestern University, 2225 North Campus Drive, Evanston, IL 60208, USA

Received 14 December 1998; received in revised form 1 February 1999

Abstract

This paper examines the room-temperature microstructure and mechanical properties of dispersion-strengthened-cast magnesium (DSC-Mg) containing 30 vol.% of 0.33 μm yttria dispersoids. The dispersoids are reasonably well distributed in both cast and extruded materials and the extruded matrix grains size is about 0.88 μm , in agreement with existing models on grain pinning. The Young's modulus measured ultrasonically agrees well with the prediction of the Eshelby composite model. Premature failure in tension is observed in extruded DSC-Mg, due to casting porosities. In compression, strain softening after yield is observed in extruded DSC-Mg, which may be explained by the tension/compression asymmetry in wrought magnesium materials. Both cast and extruded DSC-Mg are much stronger in compression than most existing magnesium alloys and composites. The strengthening contributions from the dispersoids, grain boundaries and thermal mismatch dislocations are discussed. © 2000 Published by Elsevier Science S.A. All rights reserved.

Keywords: Magnesium; Oxide-dispersion-strengthening; Composites; Mechanical properties; Compressive testing; Strengthening mechanisms

1. Introduction

Magnesium alloys are attractive for applications in the automobile and aerospace industry because of their very low density as compared to other structural metals, and because of their high stiffness, strength and conductivity as compared to polymers [1,2]. However, because of their rapid loss of strength at temperatures above ambient and their poor creep resistance at elevated temperatures, magnesium alloys are rarely used above 190°C (half the melting point), unlike aluminum alloys with a similar melting range. While magnesium matrix composites reinforced with particulates [3–5] and short fibers [6] show improved creep resistance, dispersion-strengthening holds the highest potential for improvement of high-temperature properties of magnesium, as shown in many other metal systems [7,8].

Oxide-dispersion-strengthened magnesium (ODS-Mg) has been manufactured in the past by powder metallurgy, which is a very challenging process given the reactive and pyrophoric nature of magnesium powders. Thus, only few investigations exist on creep behavior of ODS-Mg: Mg-0.5Zr/0.05 vol.% MgO fabricated by extrusion of cold-compacted powders [9], Mg/1 vol.% MgO produced by extrusion of sintered powders [10], and Mg/0.11 vol.% MgO fabricated by powder metallurgy and extrusion techniques [11,12]. A recent alternative processing technique for ODS-metals with high volume fractions (larger than about 20 vol.%) of relatively coarse oxide dispersoids (larger than about 0.25 μm) is liquid metal pressure infiltration of a ceramic particle preform, first demonstrated for dispersion-strengthened-cast aluminum (DSC-Al) containing 25 vol.% of 0.28 μm alumina dispersoids [13–15]. This process has been recently extended to magnesium containing high volume fractions of submicron oxide dispersoids (DSC-Mg) [16]. The purpose of the present article is to report on the microstructure and room-temperature mechanical properties of DSC-Mg containing high volume fractions of yttria dispersoids.

* Corresponding author. Tel.: +1-847-491-5370; fax: +1-847-467-6573.

E-mail address: dunand@nwu.edu (D.C. Dunand)

2. Materials and experimental procedures

The DSC-Mg material used in the present investigation was fabricated by Chesapeake Composites Corp. (Newcastle, DE) by liquid metal pressure-infiltration of unalloyed magnesium into a preform consisting of 30 vol.% unsintered submicron Y_2O_3 particles. Yttria was chosen as reinforcement because of its thermodynamic stability with molten and solid magnesium and its availability in chemically pure form as submicron powder. As-cast DSC-Mg billets with 42.9 mm diameter were further extruded into rods with 9.5 mm diameter (extrusion ratio of 20) at a ram speed of 50 cm/min and a temperature of 400°C. Control samples of unalloyed DSC-Al containing 32 vol.% of 0.28 μm Al_2O_3 dispersoids (also from Chesapeake Composites Corp.) were also extruded with a extrusion ratio of 12.

The solidus temperature of extruded DSC-Mg was measured with a DuPont 2100 Thermal Analysis unit with a heating rate of 10°C/min. up to 760°C under flowing argon. Sample density was measured in de-ionized water according to Archimedes' principle at room temperature, using the temperature dependence of water density given in Ref. [17]. In order to avoid corrosion, DSC-Mg was immersed in water for less than 5 min. As a comparison, DSC-Mg density was also measured in ethyl phthalate ($C_{12}H_{14}O_4$), with a temperature dependence of density given in Ref. [18], which was chosen because of its low surface tension, high viscosity, low vapor pressure, and lack of reactivity with magnesium.

The microstructure of DSC-Mg was examined using a Hitachi H700 transmission electron microscope (TEM) operating at 200 kV. TEM samples were cut along the extruded direction for extruded DSC-Mg and the solidification direction for cast DSC-Mg and ground to a thickness of about 50 μm . Disks with a diameter of 3 mm were punched and further dimpled and polished to a thickness of about 20 μm . Thinning to perforation was performed on a Precision Ion Polishing System (Gatan Model 691) with a voltage of about 4 keV, a current of 20 μA , and a gun angle of 6°. Fracture surfaces were observed using a Hitachi S-570 scanning electron microscope (SEM) operating at 20 kV.

Samples for dynamic measurements of Young's modulus were cut along longitudinal and transverse directions. Shear and longitudinal waves were produced by Matec quartz piezoelectric transducers operating at 5 and 50 MHz, respectively. The velocity of ultrasonic waves propagating through the samples was determined using a pulse-echo technique with a digital oscilloscope.

Cylindrical compression samples (with a diameter of 6.35 mm and a length of 12.7 mm) and dog-bone tension samples (with a gage diameter of 6.35 mm and a gage length of 25.4 mm) were machined along the

extrusion direction for extruded DSC-Mg and the solidification direction for cast DSC-Mg. Compression tests were performed at a cross-head velocity of 0.02 mm/min in a compression cage to insure uniaxial deformation, which was outfitted with WC-Co platens and an extensometer measuring the cross-head displacement. The elastic deformation of the cross-head with the cage was measured without sample and subtracted from all experimental compression stress–strain curves. Tensile tests were performed on a MTS Sintech 20/G at a cross-head velocity of 1 mm/min using an extensometer on the gage section.

3. Experimental results

3.1. Microstructure

The solidus temperature of extruded DSC-Mg was measured as 644°C, very close to the melting point of pure Mg of 651°C [19]. The density of extruded DSC-Mg, measured separately in the two types of liquids, was the same within error, $\rho = 2.7154 \pm 0.0024 \text{ g/cm}^3$. The volume fraction of yttria was then estimated to be $f = 0.297 \pm 0.001$, assuming no porosity and using densities of pure magnesium of 1.74 g/cm^3 and yttria of 5.03 g/cm^3 [20]. The density of extruded DSC-Al was measured as $\rho = 3.1005 \pm 0.0005 \text{ g/cm}^3$, corresponding to a volume fraction $f = 0.316 \pm 0.001$.

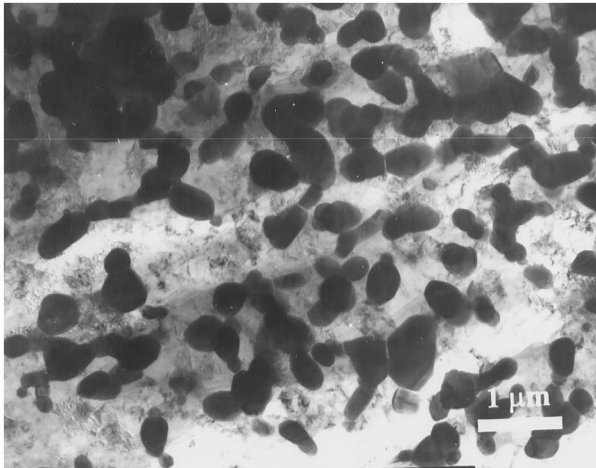
Polished metallographic cross-sections of the extruded DSC-Mg rod revealed the presence of about 20 small pores (ca. 1–2 μm in diameter) near the center of the extruded rod, which were identified as casting defects that were not fully closed during extrusion. The surface fraction of these pre-existing porosities was very small, less than 0.01%. No macroscopic particle-free areas were observed by TEM in DSC-Mg, and as shown in Fig. 1(a), yttria dispersoids are well dispersed at the microscopic level in the matrix of cast DSC-Mg. After extrusion, the distribution of yttria dispersoids is even improved (Fig. 1(b)), although some particle clusters and particle-poor areas with a size of about 1 μm are still visible.

The size of the matrix grains and the dispersoids is shown in Fig. 2(a,b) for DSC-Mg in the cast and extruded states, respectively. The average diameter of yttria particles is $d = 0.33 \pm 0.03 \mu\text{m}$, based on 69 separate size measurements in TEM micrographs. The particle aspect ratio is about 1.2 (based on 40 measurements), so that particles can be considered to be near equiaxed. The matrix grain size is difficult to determine by optical microscopy because Y_2O_3 –Mg interface dissolution does not allow for matrix grain boundary etching. TEM observation of cast DSC-Mg (Fig. 2(a)) shows subgrains with a mean linear intercept of $\bar{L} = 0.47 \pm 0.08 \mu\text{m}$, based on eight measurements.

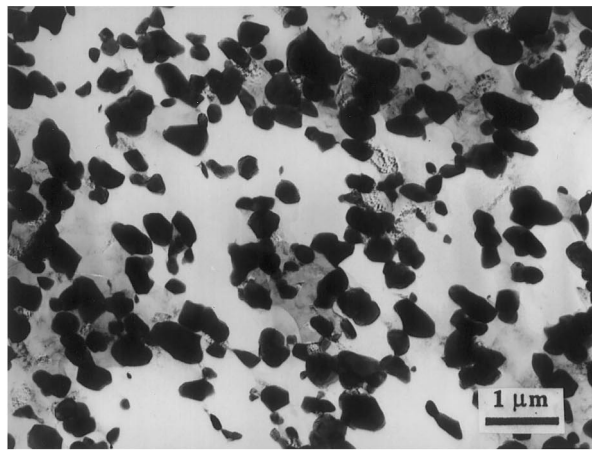
Directional solidification is expected to give very large grains, as observed for as-cast DSC-Al [13]. On the other hand, as illustrated in Fig. 2(b), TEM micrographs show high-angle grain boundaries in extruded DSC-Mg with a mean linear intercept of $\bar{L} = 0.50 \pm 0.26 \mu\text{m}$ for 15 grains, taken as the average of the largest and smallest grain dimension on the TEM projection. Assuming that \bar{L} is equal to the value of the mean linear intercept of random lines, an average spatial grain diameter $D = 1.75 \times \bar{L} = 0.88 \pm 0.46 \mu\text{m}$ is found [21]. As expected from a recrystallized, pinned microstructure, most yttria particles are found at grain boundaries.

3.2. Mechanical properties

The Young's modulus E , Poisson's ratio ν and shear modulus G were calculated according to the following relations [22,23]:

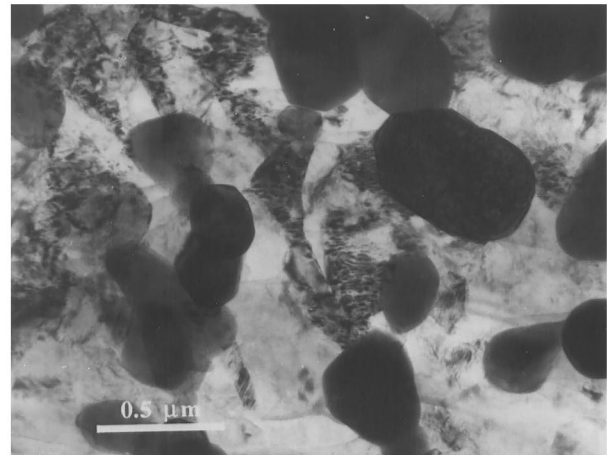


(a)

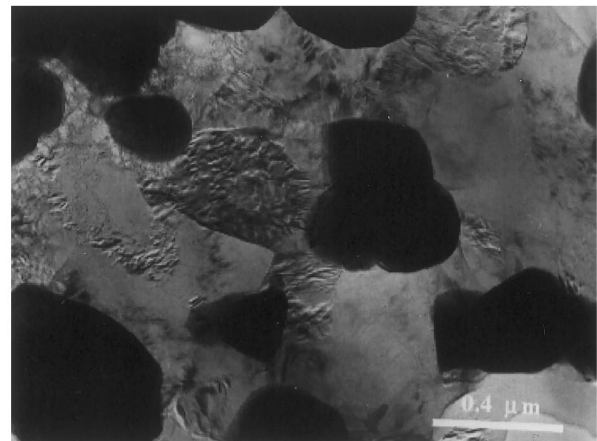


(b)

Fig. 1. TEM micrographs of (a) as-cast and (b) extruded DSC-Mg showing the distribution of submicron yttria dispersoids (black) in the magnesium matrix (white).



(a)



(b)

Fig. 2. TEM micrographs showing (a) matrix subgrains (mottled regions) and yttria dispersoids (black) for as-cast DSC-Mg and (b) matrix grains and dispersoids for extruded DSC-Mg.

$$G = \rho_s \cdot v_s^2 \quad (1)$$

$$\nu = \frac{2 - (v_l/v_s)^2}{2 \cdot (1 - (v_l/v_s)^2)} \quad (2)$$

$$E = 2 \cdot (1 + \nu) \cdot G \quad (3)$$

where ρ_s is the specimen density measured by Archimedes' method, and v_l and v_s are the longitudinal wave velocity and the shear wave velocity, respectively. Experimental elastic constants of extruded DSC-Mg are listed in Table 1.

In tension, extruded DSC-Mg failed in the elastic regime at a stress of about 230 MPa, preventing the determination of the yield and ultimate tensile stresses. The fracture surface of the tensile sample is shown in Fig. 3 and is neither fully brittle (cleavage) nor fully ductile (dimples); rather, small cavities are observed with a size of 1–2 μm , which could correspond to particle pull-out with local plastic deformation. The preexisting casting porosities are probably the reason

Table 1

Elastic constants of extruded DSC-Mg as measured by ultrasonic techniques and as predicted by theoretical models

	G (GPa)	ν (-)	E (GPa)	E (shear-lag model) (GPa)	E (Eshelby model) (GPa)
Longitudinal	23.0	0.30	59.8	49.8	64.4
Transverse	25.0	0.27	63.6	49.8	64.4

for premature failure in tension, as the high applied stresses produced large stress concentrations which could not be relieved due to the limited slip capability of HCP magnesium.

The compressive stress–strain curves of cast and extruded DSC-Mg are plotted in Fig. 4(a). For comparison, the compressive stress–strain curves of extruded DSC-Al containing about 32 vol.% alumina and of pure magnesium [24] are also given in Fig. 4(a). The grain size of extruded DSC-Al containing about 32 vol.% alumina is expected to be less than 1.3 μm , the measured grain size of extruded DSC-Al containing about 25 vol.% alumina [13].

4. Discussion

4.1. Grain size

In the development of the Zener-pinning relation on the inhibition of grain growth by second-phase particles, an estimation of the grain size D is given by Hellman and Hillert [25,26] for high volume fractions (i.e. $f > 0.1$) of particles with diameter d :

$$D = 1.8 \cdot \frac{d}{f^{1/3}} \quad (4)$$

Another estimation of the grain size is given by Humphreys et al. [27,28] for the case of recrystallization by particle-stimulated nucleation, for the case where each particle (larger than 1 μm) nucleates one grain:

$$D = d \cdot \left(\frac{1-f}{f} \right)^{1/3} \quad (5)$$

Finally, if particles block all grain growth and the inter-particle distance dictates the grain size obtained through recrystallization of the matrix during extrusion, a simple geometric argument can be used to estimate the grain size. We assume spherical particles arranged in an hexagonal lattice with an equal inter-particle distance and grains occupying the voids between the particles. Then, there are six larger grains (in octahedral voids) and 12 smaller grains (in tetrahedral voids) in the hexagonal unit cell which contains six particles [29], corresponding to three grains per particle. The larger octahedral void size and the smaller tetrahedral void size among particles is $d_{\text{ov}} = \sqrt{2} \cdot \lambda - d$

and $d_{\text{tv}} = (2/\sqrt{3}) \cdot \lambda - d$, respectively, where λ is the center-to-center distance of particles, given by $\lambda = d \cdot [\pi/(3\sqrt{2}f)]^{1/3}$. If all particles are positioned at the triple points of the recrystallized grains, the grain size can be taken as a weighted average of $(d_{\text{ov}} + d)$ and $(d_{\text{tv}} + d)$:

$$D = \frac{\sqrt{6} + 4}{3\sqrt{3}} \cdot d \cdot \left(\frac{\pi}{3\sqrt{2}f} \right)^{1/3} \approx 1.12 \cdot \frac{d}{f^{1/3}} \quad (6)$$

For DSC-Mg with 30 vol.% yttria particles, Eqs. (4)–(6) give respectively $D = 0.89$, 0.44 and 0.55 μm , in reasonable agreement with the experimental grain size of $D = 0.88 \pm 0.46 \mu\text{m}$. A slight experimental overestimate of the grain size is expected, because grains in particle-poor areas in the microstructure are easier to observe and thus bias measurements toward higher values. This bias may also explain why the measured grain size of extruded DSC-Al containing 25% alumina ($D = 1.3 \mu\text{m}$ [13]) is significantly larger than the values calculated from Eqs. (4)–(6) ($D = 0.40$ – $0.80 \mu\text{m}$): an extrusion ratio of 12 was used for DSC-Al, smaller than the value of 20 for DSC-Mg, so that more particle-poor areas exist in DSC-Al, leading to a stronger experimental bias towards large grains.

4.2. Elastic properties

As shown in Table 1, the longitudinal Young's modulus of DSC-Mg is about $E = 60 \text{ GPa}$, 34% higher than

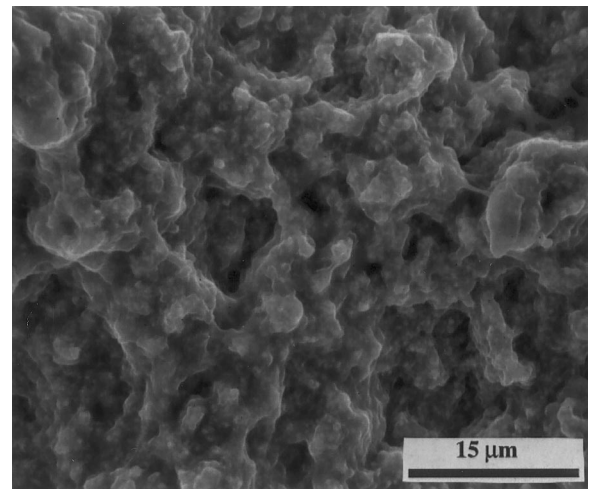


Fig. 3. SEM picture of the tensile fracture surface of extruded DSC-Mg.

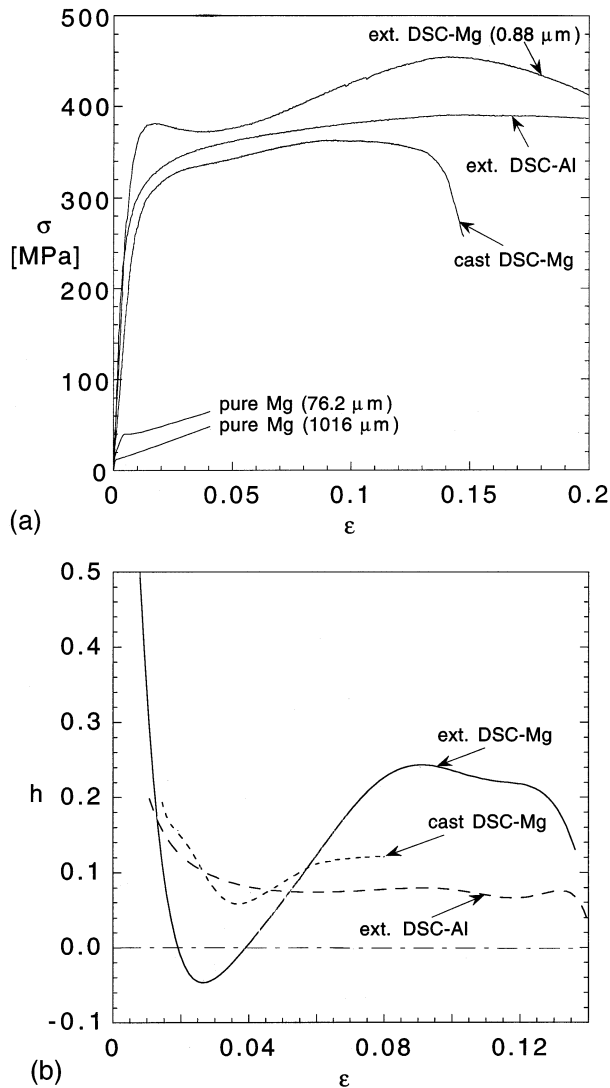


Fig. 4. (a) Stress–strain curve of pure Mg [24], DSC-Al and DSC-Mg (b) strain-hardening exponent–strain curve of DSC-Al and DSC-Mg.

that of pure magnesium ($E_m = 44.7$ GPa [24]). This experimental value is in reasonable agreement with the Young's modulus determined from the elastic slope of the tensile stress–strain curve (Table 2), $E = 65$ GPa. For comparison, the elastic modulus of DSC-Mg is calculated according to the modified shear-lag model [30] and the Eshelby model [31], using a Poisson's ratio of $\nu_m = 0.35$ for magnesium [24] and assuming a particle aspect ratio of unity. With the elastic modulus of yttria given as $E_p = 174.3$ and 179.8 GPa [32], we use an average value of $E_p = 177$ GPa and assume $\nu_p = 0.30$ for the Poisson's ratio of yttria. Table 1 shows that the shear-lag model underestimates the elastic modulus, as expected given the small particle aspect ratio, whereas the Eshelby model agrees well with experimental data of extruded DSC-Mg, as also observed in DSC-Al [13] and in metal matrix composites with larger particle size [33].

The mechanical compressive properties of DSC-Mg are compared in Table 2 to those of DSC-Al, pure magnesium, various magnesium alloys (cast, extruded or rapidly solidified), and magnesium matrix composites reinforced with SiC particles (cast or mechanically alloyed). The Young's modulus of extruded DSC-Mg is larger than those of magnesium alloys and composites with 10 vol.% SiC, similar to that of pure Mg reinforced with 20 vol.% SiC particles, and smaller than those of Mg/30 vol.% SiC and Mg6Zn/20 vol.% SiC, because of the much higher elastic modulus of SiC ($E = 420$ GPa) [20] as compared to Y_2O_3 ($E = 177$ GPa).

4.3. Plastic properties

As indicated in Table 2, the 0.2% proof compressive stress of both cast and extruded DSC-Mg materials is much higher than that of pure magnesium and magnesium alloys, but similar to that of magnesium matrix composites with 20 and 30% SiC measured in tension. Rapidly-solidified AZ91 with a grain size of 2–3 μm and large numbers of very fine precipitates has the highest proof and ultimate strengths of all magnesium materials in Table 2. However, unlike DSC-Mg, this material is not in thermodynamic equilibrium and is expected to quickly lose strength after exposure at elevated temperature.

Fig. 4(a) shows that cast DSC-Mg and extruded DSC-Al have similar proof and ultimate compressive stresses, while extruded DSC-Mg exhibits significantly higher values. Aluminum has five independent slip systems, so that recovery of secondary dislocations by annihilations during plastic deformation can easily happen at room temperature. The higher yield point of DSC-Mg may be due to the availability of only three basal slip systems of $(0001)\langle 11\bar{2}0 \rangle$ and the higher critical stress for nonbasal slip at room temperature in magnesium [24].

The strain hardening exponent ($h = \partial \ln \sigma / \partial \ln \epsilon$) is shown as a function of strain for DSC-Mg and DSC-Al in Fig. 4(b). For extruded DSC-Al, the strain hardening exponent decreases gradually with increasing strain and reaches a stable value at a strain of about 0.06. In contrast, the strain hardening exponent decreases to a minimum value at a strain of about 0.036 for cast DSC-Mg and of about 0.027 for ext. DSC-Mg and then increases gradually with strain. For extruded DSC-Mg, h takes negative values for strains between 0.02 and 0.04, corresponding to strain softening which is also observed in pure Mg with small grains (Fig. 4(a)).

Strain softening can be explained by the tension/compression asymmetry which is a well-known phenomenon in wrought magnesium [24] due to slip on basal planes in textured microstructure at room temperature. While the compressive and tensile yield strengths are equal for cast magnesium without texture, extruded

Table 2
Processing route, grain size D , particle size d and mechanical properties of DSC-Mg, DSC-Al and several other magnesium materials^a

Magnesium systems	Processing ^b	D (μm)	d (μm)	E (MPa)	$\sigma_{0.2}$ (GPa)	UTS (MPa)	Elong. (%)	Reference
<i>Pure metal</i>								
Pure Mg	Cast+extruded	–	–	45	71 ^c	192	9	[41]
Pure Mg (<99.8%)	–	76.2	–	45	43 (34)	>123 (>65)	– (–)	[24]
	–	1016	–	45	20 (13)	69 (>48)	– (–)	[24]
<i>Alloys</i>								
AZ91D	Cast	–	–	45	97 (97)	165	2.5	[46]
AZ10A	Extruded	–	–	45	145 (69)	240 (–)	10 (–)	[46]
AZ91	RS+extruded	2–3	–	–	416	486	6.2	[35]
<i>Composites</i>								
AZ91; 10% SiC	Cast	42	7	44.7	135	152	0.8	[3]
Pure Mg; 10% SiC	Cast+extruded	–	24	45	120	160	2	[47]
Pure Mg; 20% SiC	MA+extruded	–	6	66	304	350	1.0	[47]
Pure Mg; 30% SiC	MA+extruded	–	6	74	303	>303	0.2	[47]
Mg6Zn; 20% SiC	Cast+extruded+T4	10–25	3.3	73	284	396	3.4	[4]
Mg6Zn; 20% SiC	Cast+extruded+T6	10–25	3.3	73	383	427	1.2	[4]
<i>Dispersion strengthened metals</i>								
DSC-Mg; 30% Y ₂ O ₃	Cast	–	0.33	–	(268)	(363)	(15)	Present work
DSC-Mg; 30% Y ₂ O ₃	Cast+extruded	0.88	0.33	65	>230 ^d (344)	>230 ^d (455)	0 ^d (>20)	Present work
DSC-Al; 32% Al ₂ O ₃	Cast+extruded	<1.3	0.28	–	(264)	(>389)	(>20)	Present work

^a Values in parentheses are for compressive tests.

^b RS, rapidly solidified; MA: mechanically alloyed.

^c 0.1% proof stress.

^d Samples failed prematurely in the elastic range.

magnesium alloys exhibit a yield strength which is about 47% smaller in compression than in tension (asymmetry ratio of 0.53, defined as the ratio of compressive yield stress to tensile yield stress), due to a very strong preferred grain orientation with basal planes parallel to the extrusion direction which favors $\{10\bar{1}2\}$ twinning in compression but not in tension. For artificially aged extruded magnesium alloys, the texture is a little bit weaker such that the compressive yield stress is 18% smaller than the tension yield stress (asymmetry ratio of 0.82) [24]. For extruded high-purity magnesium [34], the compressive yield stress is about 40% lower than the tensile yield stress and an apparent steady-state stress stage with several small stress-drop stages is observed in compressive curves.

The tension/compression asymmetry is also affected by grain size: for example, the asymmetry ratio increases from 0.68 to 0.79 as the grain size decreases from 1016 to 76 μm in polycrystalline magnesium [24]. Furthermore, texture and twinning were not detected in some fine-grained magnesium materials, for example in rapidly-solidified (RS) AZ 91 Mg alloys with grain sizes of 2–3 μm [35] and 1.2 μm [36].

For our extruded fine-grained DSC-Mg, the tension/compression asymmetry, if it exists, should be much

smaller than for conventional extruded magnesium due to fine grains and extensive recrystallization around particles [27]. However, as also shown in DSC-Al [13], recrystallization probably did not totally eliminate the extrusion texture so that basal planes could be oriented parallel to the extrusion direction in extruded DSC-Mg. In that case, compressive deformation of extruded DSC-Mg should consist of both micro-twinning and basal slip at the early stage of plastic deformation. As micro-twinning takes place, textured basal slip systems gradually adjust their orientations to deviate from the extrusion direction and start to slip such that dislocations annihilate and strain softening occurs. When all textured basal planes become randomly distributed due to micro-twinning, the load drops to its minimum and as basal slip becomes gradually dominant, strain hardening increases.

Because of directional solidification, as-cast DSC-Mg should also exhibit some texture, which is, however, expected to be much weaker than in extruded DSC-Mg. As expected, the drop in strain hardening exponent is much less in cast DSC-Mg than in extruded DSC-Mg (Fig. 4a,b). Finally, extruded DSC-Al has enough slip systems for plastic deformation, so that dislocation slip is always dominant and twinning does not take place.

As shown in Fig. 4(b), the strain hardening in DSC-Al reaches a stable level without the intermediate drop shown by DSC-Mg.

4.4. Yield strength in DSC-Mg

We now discuss the yield stress of DSC-Mg in the light of traditional strengthening mechanisms for metals [28,37], as done for DSC-Al with 25% Al₂O₃ in a previous publication [13]. Without solid-solution or precipitate strengthening in the unalloyed matrix, the three main strengthening mechanisms are: (1) forest hardening from dislocations produced by the difference in thermal expansion between matrix and reinforcement; (2) fine-grain strengthening, due to grain-boundaries blocking dislocations; and (3) Orowan strengthening due to the interaction of dislocations with fine particles. These three contributions are estimated for DSC-Mg in the following.

Dislocations with density ρ_{th} , which are created from the relaxation of thermal expansion mismatch between the matrix and the reinforcing particles, may cause an increase in yield stress which is expressed as:

$$\sigma_{CTE} = A \cdot M \cdot G \cdot b \cdot \rho_{th}^{1/2} \quad (7)$$

where $M = 6.5$ [38] is the mean matrix orientation factor for magnesium and the constant $A = 0.2$ characterizes the transparency of the dislocation forest for basal–basal dislocation interaction in magnesium at 300 K [39]. The Burgers vector and the shear modulus are taken as $b = 3.21 \times 10^{-10}$ m and $G = 16.6$ GPa [19], respectively. In Equation (7), the dislocation density ρ_{th} can be estimated by assuming that dislocation loops of radius $d/\sqrt{2}$ are punched by spherical particles with volume fraction f to relax the thermal mismatch due to the difference in thermal expansion coefficients $\Delta\alpha$ for a temperature excursion ΔT [40]:

$$\rho_{th} = \frac{12\sqrt{2} \cdot \Delta\alpha \cdot \Delta T \cdot f}{b \cdot d \cdot (1 - f)} \quad (8)$$

The average thermal expansion coefficients of pure magnesium and yttria are $2.7 \times 10^{-5} \text{ K}^{-1}$ from 293 to 573 K [41] and $7.5 \times 10^{-6} \text{ K}^{-1}$ from 298 to 600 K [42], respectively. Taking a temperature excursion $\Delta T = 250$ K (corresponding to a stress-free homologous temperature of 0.6), Eq. (7) predicts $\sigma_{CTE} = 126$ MPa.

The second strengthening mechanism is described by the Hall–Petch relation [37]:

$$\sigma_{HP} = K/D^{1/2} \quad (9)$$

where D is the grain size and K is given by Ref. [35] as $210 \text{ MPa} \cdot \mu\text{m}^{1/2}$ for seven extruded RS AZ91 alloys with

grain sizes from 0.3 to 3.7 μm and two conventionally cast AZ91 alloys with large grain sizes of 30 μm and 5 mm. However, reanalyzing their data shows one best-fit value of $K = 166 \text{ MPa} \cdot \mu\text{m}^{1/2}$ for the full range of grain sizes (nine data points from 0.3 μm to 5 mm) and another best-fit value of $K = 133 \text{ MPa} \cdot \mu\text{m}^{1/2}$ for extruded RS AZ91 (seven data points from 0.3 to 3.7 μm). Using the latter value, Eq. (9) predicts $\sigma_{HP} = 115\text{--}205$ MPa for extruded DSC-Mg with a grain size of $D = 0.88 \pm 0.46$ μm .

Third, the interactions between dislocations and fine particles result in an increase of yield stress given by the Orowan stress [43]:

$$\sigma_{Or} = M \cdot \frac{0.4 \cdot G \cdot b}{\pi \cdot \bar{\lambda}} \cdot \frac{\ln(\bar{d}/b)}{\sqrt{1 - \nu_m}} \quad (10)$$

where $\bar{d} = \sqrt{2/3}d$, and $\bar{\lambda}$ is the mean inter-particle distance given by $\bar{\lambda} = \bar{d}(\sqrt{\pi/4f} - 1)$. Eq. (10) gives $\sigma_{Or} = 218$ MPa for DSC-Mg.

An upper-bound for the tensile yield stress is given by the sum of the individual strengthening mechanisms and a Peierls stress (assumed to be about 5 MPa, see Appendix A). For compression yield stress, this upper-bound should be multiplied by the asymmetry ratio, which is unknown for DSC-Mg. We assume a value of 0.75 for extruded DSC-Mg, the average value of extruded magnesium alloys from Ref. [24]. For cast DSC-Mg, directional solidification induced some texture, as seen in the strain softening in Fig. 4(a), so we assume a value of 0.85 for the asymmetry ratio, between the value for extruded DSC-Mg and the value of unity for texture-free magnesium. In as-cast DSC-Mg, grain-boundary strengthening is ignored because of the very coarse grains expected for directional solidification, and so is any strengthening due to subgrains. The predicted compressive yield stress upper bounds are then $\sigma_y = 348\text{--}416$ MPa for extruded DSC-Mg and $\sigma_y = 297$ MPa for cast DSC-Mg. These values are reasonably close to the experimental proof stresses of $\sigma_{0.2} = 344$ MPa for extruded DSC-Mg and $\sigma_{0.2} = 268$ MPa for cast DSC-Mg, given uncertainties in material parameters, grain size and dispersoid size as well as simplifying assumptions such as dispersoid spatial distribution, shape and average size.

5. Conclusions

The microstructure and mechanical properties of DSC-Mg with about 30 vol.% of 0.33 μm yttria dispersoids were investigated at room temperature. The yttria dispersoid distribution is reasonably good in cast DSC-Mg and further improved by extrusion. The matrix grains in extruded DSC-Mg are equiaxed with a size of about 0.88 μm , which is close to the value predicted by

Zener-pinning relations. The Young's modulus measured ultrasonically agrees well with the prediction by the Eshelby model, while the prediction by the shear-lag model underestimates the Young's modulus. In tension, failure occurs in the elastic region, most probably because of pre-existing processing porosities in extruded DSC-Mg. In compression, DSC-Mg is stronger than conventionally-processed magnesium alloys and most magnesium matrix composites. Extruded DSC-Mg exhibits strain softening, which may be explained by the tension/compression asymmetry in wrought magnesium materials. The contribution of three strengthening mechanisms to the yield strength in DSC-Mg are estimated: Orowan strengthening is the main contributor to the strength of cast DSC-Mg, while Hall–Petch strengthening is also substantial in fine-grained, extruded DSC-Mg.

Acknowledgements

This work was supported by National Science Foundation, under Grant No. DMR 9417636, monitored by Dr B. McDonald. The authors gratefully acknowledge Dr W.A. Chiou for assistance in TEM operation.

Appendix A. Calculation of Peierls stress in magnesium

The theoretical value of τ_p may be estimated from the expression of Hull and Bacon [44]:

$$\tau_p = \frac{2G}{(1-\nu)} \exp\left(-\frac{2\pi w}{b}\right) \quad (\text{A1})$$

where $w = a/(1-\nu)$ for an edge dislocation (with the inter-planar spacing of a), $\nu = 0.35$, $b = 0.321$ nm and $G = 16.6$ GPa at 298 K for magnesium [19]. For the $\{10\bar{1}0\}$ prismatic planes in magnesium, $a = 0.37$ nm [45]. Eq. (A1) then gives a shear stress value of $\tau_p = 0.74$ MPa, corresponding to a tensile Peierls stress of polycrystalline magnesium $\sigma_p = M \times \tau_p = 4.8$ MPa.

References

- [1] R.F. Decker, Adv. Mater. Proc. 154 (1998) 31.
- [2] F.H. Froes, D. Eliezer, E. Aghion, JOM 50 (1998) 30.
- [3] A. Luo, Metal. Mater. Trans. 26A (1995) 2445.
- [4] A. Martin, J. Llorca, Mater. Sci. Eng. A201 (1995) 77.
- [5] P.E. Holden, R. Pilkington, G.W. Lorimer, in: G.W. Lorimer (Ed.), Proceedings of the Third International Magnesium Conference, The Institute of Materials, 1996, p. 647.
- [6] B.L. Mordike, P. Lukac, in: G.W. Lorimer (Ed.), Proceedings of the Third International Magnesium Conference, The Institute of Materials, 1996, p. 419.
- [7] E. Arzt, Res. Mech. 31 (1991) 399.
- [8] S. Ochiai, Mechanical Properties of Metallic Composites, Marcel Dekker, New York, 1994.
- [9] P. Greenfield, W. Vickers, J. Nucl. Mater. 22 (1967) 77.
- [10] W. Vickers, P. Greenfield, J. Nucl. Mater. 27 (1968) 73.
- [11] K. Milicka, J. Cadek, P. Rys, Acta Metall. 18 (1970) 1071.
- [12] I.G. Crossland, R.B. Jones, Met. Sci. J. 6 (1972) 162.
- [13] A.M. Redsten, E.M. Klier, A.M. Brown, D.C. Dunand, Mater. Sci. Eng. A201 (1995) 88.
- [14] A.M. Brown, E.M. Klier, US Patent 5,511,603 (1996).
- [15] A.M. Brown, E.M. Klier, US Patent 5,702,542 (1997).
- [16] E.M. Klier, A.M. Brown, NSF Report DMI-9302463 (1996).
- [17] D.W. Green, J.O. Maloney, Perry's Chemical Engineer's Handbook, McGraw-Hill, New York, 1984, p. 3.
- [18] T.E. Daubert, R.P. Danner, Physical and Thermodynamic Properties of Pure Chemicals: Data Compilation, Part 1, Taylor and Francis, London, 1993.
- [19] H.J. Frost, M.F. Ashby, Deformation-Mechanism Maps: The Plasticity and Creep of Metals and Ceramics, Pergamon, Oxford, 1982, p. 44.
- [20] CRC Handbook of Chemistry and Physics, 78th edn., CRC Press, Boca Raton, FL, 1997, p. 2512.
- [21] A. Ball, M.M. Hutchison, Metal Sci. J. 3 (1969) 1.
- [22] E. Schreiber, O.L. Anderson, N. Soga, Elastic Constants and their Measurement, McGraw-Hill, New York, 1973.
- [23] M.H. Zimmerman, Fracture of textured iron titanate, Ph.D. thesis, 1997, Northwestern University, Evanston, IL.
- [24] C.S. Roberts, Magnesium and its Alloys, Wiley, New York, 1960, p. 81.
- [25] P. Hellman, M. Hillert, Scand. J. Metals 4 (1975) 211.
- [26] M. Hillert, Acta Metall. 36 (1988) 3177.
- [27] F.J. Humphreys, W.S. Miller, M.R. Djazeb, Mater. Sci. Technol. 6 (1990) 1157.
- [28] F.J. Humphreys, A. Basu, M.R. Djazeb, in: N. Hansen, et al. (Eds.), Metal Matrix Composites—Processing, Microstructure and Properties, Risø National Laboratory, Roskilde, 1991, p. 51.
- [29] M.A. Meyers, K.K. Chawla, Mechanical Metallurgy Principles and Applications, Prentice-Hall, Englewood Cliffs, NJ, 1984, p. 215.
- [30] V.C. Nardone, K.M. Prewo, Scripta Metall. 20 (1986) 43.
- [31] T.W. Clyne, P.J. Withers, An Introduction to Metal Matrix Composites, Cambridge University Press, Cambridge, 1993, p. 44.
- [32] R.C. Anderson, in: A.M. Alper (Ed.), High Temperature Oxides: Part II Oxides of Rare Earths, Titanium, Zirconium, Hafnium, Niobium and Tantalum, Academic Press, New York, 1970, p. 1.
- [33] M. Taya, R.J. Arsenault, Scripta Metall. 21 (1987) 349.
- [34] J.W. Christian, S. Mahajan, Prog. Mater. Sci. 39 (1995) 1.
- [35] G. Nussbaum, P. Sainfort, G. Regazzoni, H. Gjestland, Scripta Metall. 23 (1989) 1079.
- [36] D. Lahaie, J.D. Embury, M.M. Chadwick, G.T. Gray, Scripta Metall. Mater. 27 (1992) 139.
- [37] W.S. Miller, F.J. Humphreys, Scripta Metall. Mater. 25 (1991) 33.
- [38] R. Armstrong, L. Codd, R.M. Douthwaite, N.J. Petch, Phil. Mag. 7 (1962) 45.
- [39] F.F. Lavrentev, Mater. Sci. Eng. 46 (1980) 191.
- [40] D.C. Dunand, A. Mortensen, Acta Metall. Mater. 39 (1991) 127.
- [41] E.F. Emley, Principles of Magnesium Technology, Pergamon, Oxford, 1966, p. 736.
- [42] Y.S. Touloukian, Thermophysical Properties of High Temperature Solid Materials, Purdue University, 1967.
- [43] L.M. Brown, R.K. Ham, in: A. Kelly, R.B. Nicholson (Eds.), Strengthening Methods in Crystals, Elsevier, Amsterdam, 1971, p. 9.
- [44] D. Hull, D.J. Bacon, Introduction to Dislocations, Pergamon, Oxford, 1984.
- [45] S.S. Vagarali, T.G. Langdon, Acta Metall. 29 (1981) 1969.
- [46] ASM Handbook, Vol. 2, Properties and Selection: Nonferrous Alloys and Special-Purpose Materials, ASM International, 1990, p. 480.
- [47] M.R. Krishnadev, R. Angers, C.G.K. Nair, G. Huard, JOM, August (1993) 52.